Visual Servo Control for Dynamic Hovering of an Underwater Biomimetic Vehicle-Manipulator System by Neural Network*

Rui Wang

Institute of Automation, Chinese Academy of Sciences
University of Chinese Academy of Sciences
Beijing, China
rwang5212@ia.ac.cn

Yu Wang, Shuo Wang, Chong Tang, and Min Tan

Institute of Automation, Chinese Academy of Sciences
Beijing, China
{yu.wang,shuo.wang,tangchong2014,min.tan}@ia.ac.cn

Abstract— This paper deals with the problem of dynamic hovering of a bio-inspired robot with undulatory fins. First, the mechanism and dynamic model of the underwater robot named RobCutt-II is briefly introduced. Next, an neural network visual servo control is presented to achieve hovering control. In particular, a dual-loop visual hovering control is designed. At first, we analyze the relationship between the image feature error and the direction of the controllable velocity. In the outer loop, a PID controller is used to calculate the current controllable velocity based on image feature error in real time. Meanwhile, the inverse model of undulatory fins is established using the neural network. The velocity error is hereby mapped to the control parameters of the undulatory fins of the RobCutt-II. The simulation results of dynamic hovering are provided to illustrate the validity of the proposed method.

Index Terms— Dynamic hovering, visual servo control, undulatory fin, image feature, neural network.

I. Introduction

Ocean is the main resource of the energy and chemical balance that sustains mankind. As an effective working platform for the implementation of marine exploration, resource development, underwater equipment maintenance, underwater rescue and other military and civilian tasks in complex water environment, underwater vehicle-manipulator systems (UVMSs) have always been the concern of the marine powers [1], [2].

Although traditional axial propeller propulsion systems can produce a strong thrust, their noise are large and their small thrust control ability are weak. Furthermore, axial propeller is easy to cause underwater dust, which affects the visual observation. Some marine animals of the order Sepiida like cuttlefish swim using flexible long fins. They have flexible maneuverability, strong anti-disturbance ability. Specially, they are good at swimming in narrow space at low speed. By imitating these fish, we can develop underwater robots propelled by undulatory fins, which would help handle the challenging problems of dynamic hovering under flow disturbance [3], [4].

Maintaining a fixed position and attitude is a critical capability for UVMSs in underwater survey and intervention missions. In particular, Dynamic hovering mode has been reported to take 35% of the total work done in a typical subsea task [5]. This ability is often taken for granted in land-based robotics because of the ease of implementation. However, an UVMS must deal with unknown currents and forces which can cause its position to change undesirably.

Visual servo control for dynamic hovering has been used in some aircrafts and underwater vehicles [6]−[9]. For example, Chen et al. developed a vision-based fuzzy controller for quadrotor tracking a ground targert [6]. Lots et al. introduced a 2-D visual servoing technique for the station keeping of an unmanned underwater vehicle with respect to planar unmarked objects on the sea bed. A linear PID controller is used to achieve slow and stable hover capabilities [8]. However, most researchers designed hovering control algotithm for the underwater vehicles equipped with traditional axial propellers. Moreover, they are mostly aimed at full-actuated systems.

However, in low-speed underwater motions such as hovering, the axial propeller is in non-full rotation working state, when the efficiency of the propulsion system is significantly reduced and the unpredictable fluid pulse could be produced. In this paper, an underwater biomimetic vehicle-manipulator system (UBVMS, named RobCutt-II) propelled by undulatory fins is introduced. Then, a neural network visual servo control for dynamic hovering of RobCutt-II is proposed, which is conductive to stable and effective underwater operations. Specifically, we design a dual-loop visual hovering controller. The input of the outer loop is the desired image feature, while the output is the desired controllable velocity. The inner loop is the velocity loop, where a neural network is used to establish the inverse model of undulatory fins. In the end, we investigate the efficacy of the proposed control through some simulation studies.

In the remainder of this paper, the modeling of the RobCutt-II is described in Section II. Sections III presents the development of the neural network visual hovering control. Simulation studies are presented in Sections IV. Finally, conclusions are given in Section V.
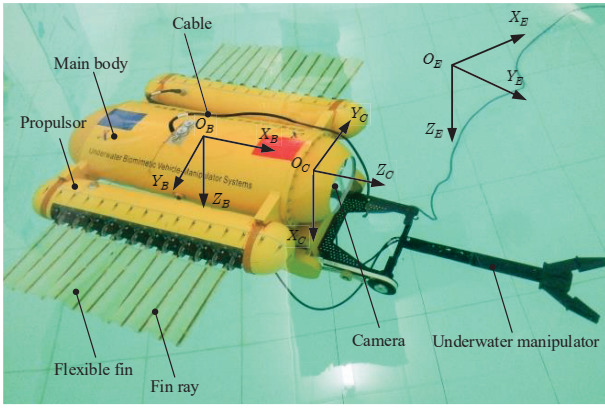
Fig. 1.   RobCutt-II prototype.

Fig. 2.   The control block diagram of hovering control.

Fig. 3.   The schematic diagram of inverse model identification by neural network.

II. MODELING OF THE ROBCUTT-II

The RobCutt-II considered in this paper is seen in Fig. 1, which consists of three parts, i.e. a main body, a five degrees of freedom manipulator and two modular propulsors with undulatory fins [10]. The camera is installed in the front of the main body. The five degrees of freedom manipulator has been detailed in [11]. Moreover, the description about the propulsor can be seen in [12].

The general dynamic model of underwater vehicles can be represented as (1) under some assumptions [13].

$$
\begin{aligned}
\dot{\eta} &= J(\psi)\nu \\
M\dot{\nu} &= -C(\nu)\nu - D\nu + \tau + \tau_d
\end{aligned} \tag{1}
$$

where $\eta = [x, y, z, \psi]^T \in \mathbb{R}^4$ represents the position and heading of the RobCutt-II, $\nu = [u, v, w, r]^T \in \mathbb{R}^4$ is the body-fixed velocity, $\tau = [\tau_u, 0, \tau_w, \tau_r]^T \in \mathbb{R}^4$ is the propulsive force and torque produced by two long fins, $\tau_d = [\tau_{du}, \tau_{dv}, \tau_{dw}, \tau_{dr}]^T \in \mathbb{R}^4$ denotes the disturbance acting on surge, sway, heave, and yaw dynamics. The definitions of the other symbols and parameters can be found in [14], [15].

Note that the actual control inputs of the RobCutt-II are the parameters of propagating waves on bilateral fins. Specifically, they include the left fin frequency, the right fin frequency, the amplitude of waves, the phase difference and the deflection angle, which are denoted by F_L, F_R, A, φ, θ_B. The relations between propulsive force or torque and the parameters of the propagating wave are derived by the experiments of three basic motions, including the forward/backward swimming, the diving/floating, and turning maneuver [16]. For example, it is known from the experiments that the surge force τ_u is proportional to the sum of the frequency of two long fins within a certain range. While the heave force τ_w is proportional to the absolute value of the sum of the frequency.

Therefore, the following equations are used to fit the characteristic curves between the propulsive force or torque and the control parameters of the undulatory fins:

$$
\tau_u = k_{u1} \frac{1 - e^{-k_{u2}A}}{1 + e^{-k_{u2}A}} \frac{1 - e^{-k_{u3}\varphi}}{1 + e^{-k_{u3}\varphi}}(F_L + F_R) \tag{2}
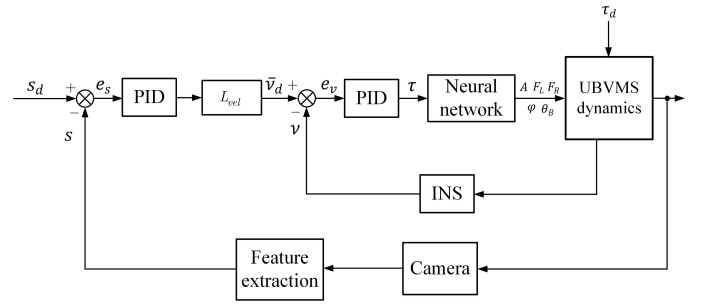$$
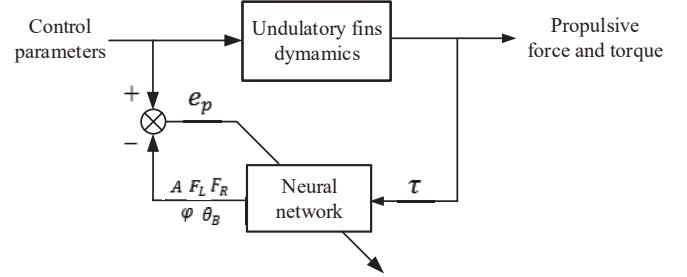
$$
\tau_w = k_{w1} \frac{1}{1 + e^{-k_{w2}(\varphi_{\max} - \varphi)}} \frac{1 - e^{-k_{w3}\theta_B}}{1 + e^{-k_{w3}\theta_B}} |F_L + F_R| \tag{3}
$$

$$
\tau_r = k_{r1} \frac{1 - e^{-k_{r2}A}}{1 + e^{-k_{r2}A}} \frac{1 - e^{-k_{r3}\varphi}}{1 + e^{-k_{r3}\varphi}}(F_L - F_R) \tag{4}
$$

where $F_L \in [-1.5, 1.5]$, $F_R \in [-1.5, 1.5]$, $A \in [0, 40]$, $\theta_B \in [-20, 20]$, and $\varphi \in [0, 40]$, φ_{max} denotes the maximum phase difference between the adjacent fins, k_{u1}, k_{u2}, k_{u3}, k_{w1}, k_{w2}, k_{w3}, k_{r1}, k_{r2}, k_{r3} are some characteristic parameters.

III. NEURAL NETWORK VISUAL HOVERING CONTROL DEVELOPMENT

A. Dual-loop Visual Hovering Control Design

The control block diagram of the dual-loop visual hovering is shown in Fig. 2. First, three coordinate systems are established as shown in Fig. 1, including the inertial coordinate system $O_E X_E Y_E Z_E$, the body-fixed coordinate system $O_B X_B Y_B Z_B$, and the camera coordinate system $O_C X_C Y_C Z_C$. In particular, we can rotate the body-fixed coordinate system by $\psi = -180°$ about Z_B axis, and then by $\theta = -90°$ about the new Y_B axis to get the camera coordinate system.

Define and select image feature $s = [x_g, y_g, a]$. (x_g, y_g), a represent the center of gravity and the area of the target object in the normalized image plane, respectively. e_s denotes the image feature error between the desired image feature s_d and real-time image feature acquired from the camera. The goal of the visual servo hovering control is to make $e_s = s - s_d$ converge to zero. Note that the RobCutt-II is an underactuated vehicle, because it can't generate a lateral motion voluntarily. Thus, the controllable velocity $\bar{\nu}$ includes
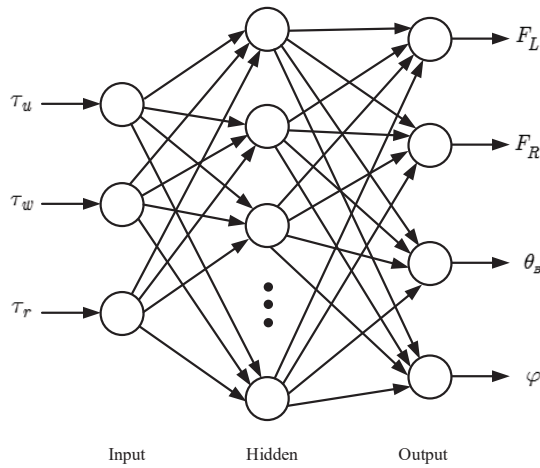
Fig. 4. Neural network structure diagram.

the velocity or angular velocity in surge, in heave, and in yaw. Then, we can calculate the desired controllable velocity $\bar{\nu}_d$ using a PID controller and the velocity direction transform matrix (VDTM) L_{vel}. The inner loop of the controller is the velocity loop, which takes the velocity error e_v as input and outputs the required propulsive force and torque τ to regulate the velocity of the vehicle to the desired one. Furthermore, an artificial neural network is utilized to map the propulsive force and torque to the control parameters of the undulatory fins. Thus the image feature error can be convergent, which means the RobCutt-II would reach the desired posture and hover stably.

The VDTM establishes the relationship between image feature error and the direction vector of the controllable velocity. Specifically, the propulsor should produce a positive surge propulsive force to make the RobCutt-II close to the target when the actual image area is smaller than the desired image area. Heave velocity along the negative Z_B-axis should be produced when x_g is smaller than the desired one. Moreover, a positive angular velocity around Z_B-axis should be produced when y_g is smaller than the desired one. Thus, we can get:

$$\bar{\nu}_d = L_{vel}\left(K_p e_s + K_d \dot{e}_s + K_i \int e_s dt\right) \tag{5}$$

with

$$L_{vel} = \begin{bmatrix} 0 & 0 & 1 \\ -1 & 0 & 0 \\ 0 & 1 & 0 \end{bmatrix} \tag{6}$$

where K_p, K_i, K_d represent the out-loop PID control parameters matrix.

B. Neural Network Inverse Model Identification of the Propulsor

In the actual control, we need to use the inverse model of the dynamic model of the undulatory fins in Section II-B, whose derivation is cumbersome. Thus we use the neural network to simulate the inverse model of the propulsor with undulatory fins. Fig. 3 shows the schematic diagram of inverse model
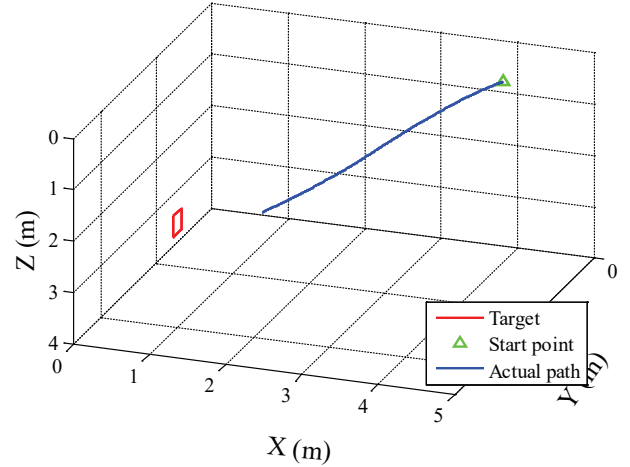

Fig. 5. Actual trajectory of the RobCutt-II during hovering control.

TABLE I
MODEL PARAMETERS OF THE ROBCUTT-II

m_{11}	m_{22}	m_{33}	m_{44}	d_{11}	d_{22}	d_{33}	d_{44}	
57.5	61.3	61.3	1.15	53	58	70	3.1	
k_{u1}	k_{u2}	k_{u3}	k_{w1}	k_{w2}	k_{w3}	k_{r1}	k_{r2}	k_{r3}
10	0.1	0.1	10	0.1	0.1	5	0.1	0.1

identification by neural network. It is seen from Fig. 3 that the output τ of the undulatory fins system is used as the input of the neural network. The output of the neural network is compared with the system input. The corresponding error e_p is used for model training, such that we can learn the dynamic inverse model of the undulatory fins.

In particular, we use the neural network structure shown in Fig. 4 to establish the mapping relationship between the propulsive force and torque and the control parameters of the undulatory fins. A three-layer feed-forward neural network (one input layer, one hidden layer, and one output layer) is utilized. Combined with the practical control experience, network structure is simplified by fixing the amplitude of undulatory fins to $36°$. Thus, the input layer has 3 nodes while the output layer has 4 nodes. The backward propagation (BP) algorithm is used to train the neural network. Hyperbolic tangent sigmoid transfer function is used as the activate function of the hidden layer and the output layer. After several tests, the optimal size of the hidden layer is selected as 10, when the error between the actual output and the desired output is small enough. Note that we can train the neural network offline and then use the trained control parameters directly in actual hovering control.

IV. SIMULATION RESULTS

In order to verify the feasibility and effectiveness of the proposed controller, we simulate the response of the RobCutt-II when the proposed neural network visual servo control is applied using the model shown in Section II. The model parameters used in the simulations are listed in Tables I.
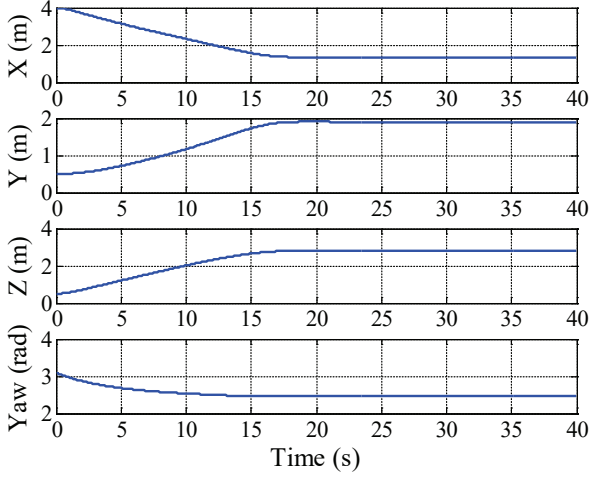
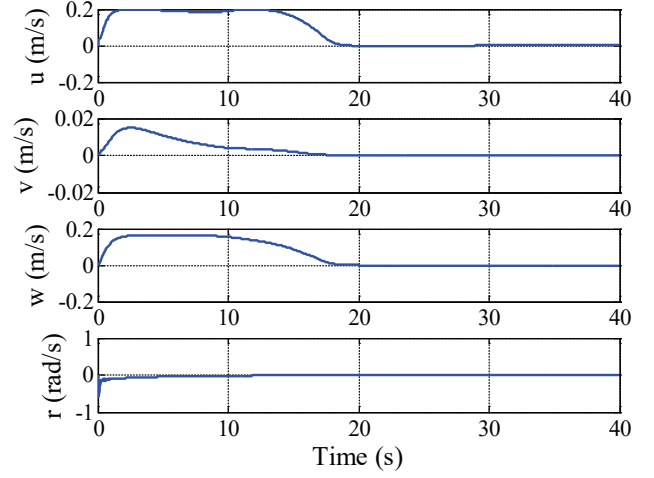Fig. 6. Time evolution of the position and heading of the RobCutt-II.

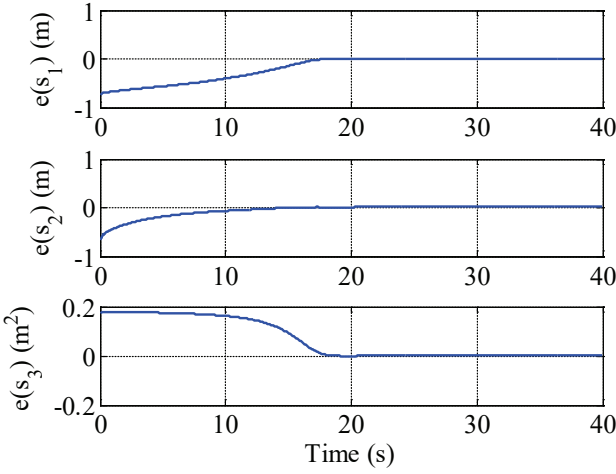Fig. 8. Time evolution of the body-fixed velocity.

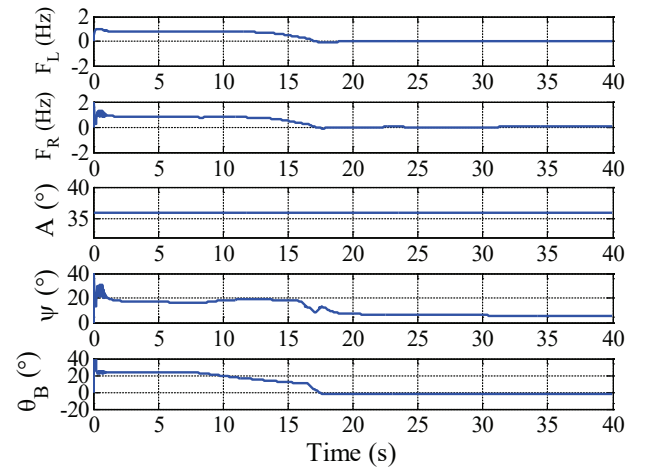Fig. 7. Time evolution of the image feature error.

Fig. 9. Time evolution of the control parameters of propagating waves on bilateral fins.

The initial states of the RobCutt-II are $(x_0, y_0, z_0, \psi_0) = (4.0\,\text{m}, 0.5\,\text{m}, 0.5\,\text{m}, \pi\,\text{rad})$, and the initial velocity is zero. The target is a $0.4\,\text{m} \times 0.3\,\text{m}$ rectangular object with center of gravity $(0.5\,\text{m}, 2.6\,\text{m}, 2.8\,\text{m})$, which is parallel with the plane $X_E O_E Y_E$ of the inertial coordinate system. The desired image feature is $s_d = (0.0\,\text{m}, 0.0\,\text{m}, 0.19\,\text{m})$. The control period is 0.05 s.

The simulation results based on these conditions are presented in Fig. 5-Fig. 9. Fig. 5 depicts the actual trajectory of the RobCutt-II in 3-D space. Fig. 6 is the time evolution of the position and heading of the RobCutt-II. Fig. 7 describes the image feature error curve. It can be seen from the figures that as the real-time image feature converges to the desired image feature, the RobCutt-II gradually reaches the desired position and heading. Fig. 8 presents the body-fixed velocity during hovering. Fig. 9 shows the time evolution of the control parameters of propagating waves on bilateral fins. Stable hovering is achieved, such that it can be concluded that the

neural network visual servo hovering control is effective.

Meanwhile, in order to verify the anti-disturbance performance of the proposed control algorithm, another simulation is performed, where zero mean Gaussian noises with standard deviation 2 are incorporated into the surge, sway, and heave dynamics of the vehicle. In addition, zero mean uniform Gaussian noise whose standard deviation is 1 is incorporated into the yaw dynamics. The initial position of the RobCutt-II is set to $(x_0, y_0, z_0) = (3.0\,\text{m}, 3.0\,\text{m}, 4.0\,\text{m})$, while the initial heading is $\pi\,\text{rad}$. Other settings are the same as these of the previous simulation.

Fig. 10 shows the trajectory of RobCutt-II under the hovering control. Fig. 11 is the time evolution of the position and heading of the RobCutt-II. Fig. 12 describes the image feature error curve. The graph reflecting time history of the body-fixed velocity is depicted in Fig. 13. Fig. 14 illustrates that the time evolution of the control parameters of propagating
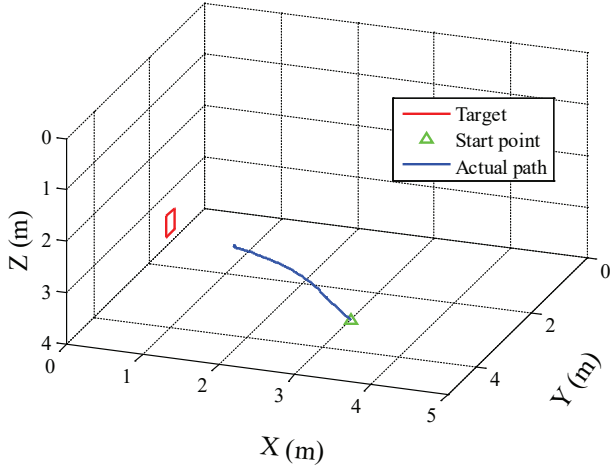
Fig. 10. Actual trajectory of the RobCutt-II during hovering control with external disturbance.
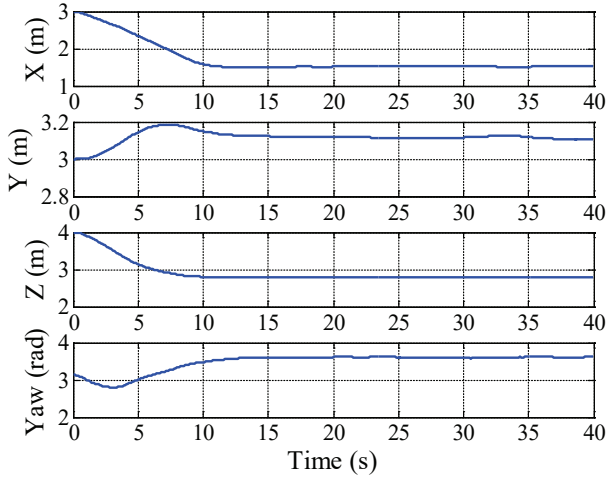

Fig. 11. Time evolution of the position and heading of the RobCutt-II.

Fig. 12. Time evolution of the image feature error.

Fig. 13. Time evolution of the body-fixed velocity.

waves on bilateral fins. It can be observed from the figures that the image error still converges to zero despite the disturbance. Moreover, although obvious fluctuations occur in the yaw angular velocity of the RobCutt-II and the frequency of two long fins, the RobCutt-II arrives at the desired position at around $15\,\mathrm{s}$ and then hovers behind the ground target stably, which demonstrates the robustness to disturbance of the proposed approach.

V. CONCLUSIONS

The closed loop hovering control of an underwater biomimetic vehicle-manipulator system has been achieved. In order to realize dynamic hovering, an dual-loop neural network visual servo control is proposed. In the outer loop, image feature error is used to calculate the desired controllable velocity using a PID controller and the velocity direction transformation matrix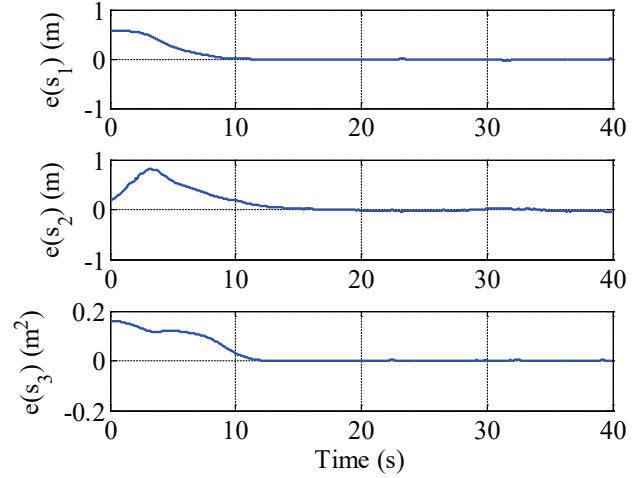. In the inner loop, the controllable velocity error is hereby mapped to the control parameters of the undulatory fins of the RobCutt-II by the neural network. The simulation results have demonstrated that the RobCutt-II can achieve dynamic hovering by the proposed controller.
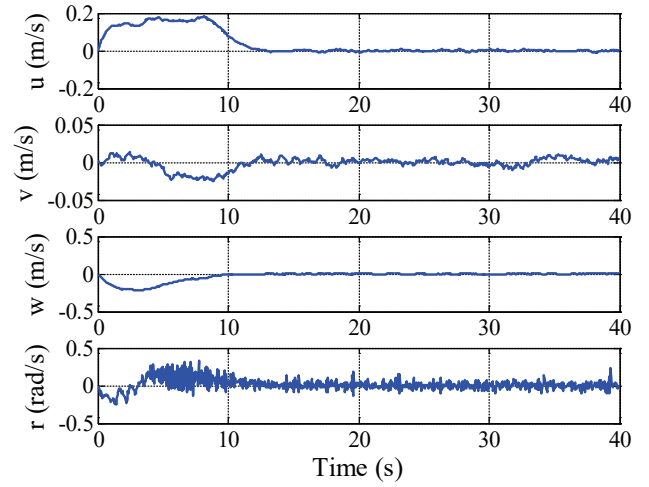
REFERENCES

[1] C. Mcfarland, M. Jakuba, S. Suman, J. Kinsey, and L. Whitcomb, "Toward ice-relative navigation of underwater robotic vehicles under moving sea ice: Experimental evaluation in the Arctic Sea," in *Proceedings of the 2015 International Conference on Robotics and Automation*, Seattle, Washington, May 2015, pp. 1527-1534.

[2] H. Shiobara, T. Kanazawa, and T. Isse, "New step for broadband seismic observation on the seafloor: BBOBS-NX," *IEEE Journal of Oceanic Engineering*, vol. 38, no. 2, pp. 396-405, 2013.

[3] Z. Wu, J. Yu, J. Yuan, and M. Tan, "Analysis and verification of a miniature dolphin-like underwater glider," *Industrial Robot: An International Journal*, vol. 43, no. 6, pp. 628-635, 2016.

[4] R. Wang, S. Wang, Y. Wang, and C. Tang, "Path following for a biomimetic underwater vehicle based on ADRC," in *Proceedings of the 2015 International Conference on Robotics and Automation*, Singapore, May 2017.
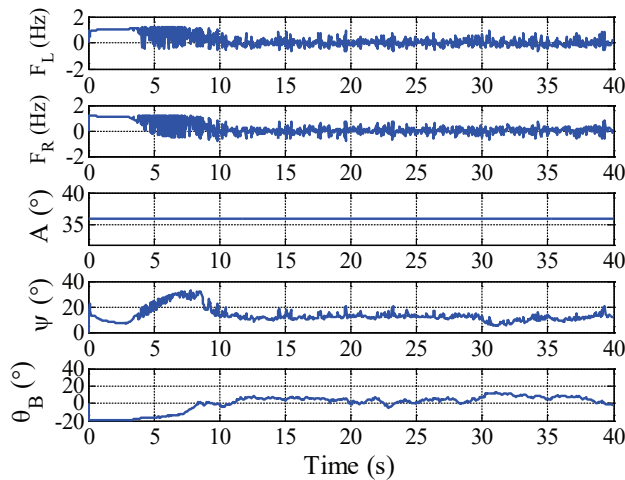
Fig. 14. Time evolution of the control parameters of propagating waves on bilateral fins.

[5] K. Goheen and E. Jefferys, "Multivariable self-tuning autopilots for autonomous and remotely operated underwater vehicles," *IEEE Journal of Oceanic Engineering*, vol. 15, no. 3, pp. 144-151, 1990.

[6] X. Chen, Z. Cao, Y. Yang, C. Zhou, and M. Tan, "Vision-based fuzzy controller for quadrotor tracking a ground target," *Advances in Science and Technology*, pp. 121-126, 2017.

[7] R. Marks, H. Wang, M. Lee, and S. Rock, "Automatic visual station keeping of an underwater robot," in *OCEANS '94. 'Oceans Engineering for Today's Technology and Tomorrow's Preservation.' Proceedings*, September 1994.

[8] J. Lots, D. Lane, and E. Trucco, "Automatic visual station keeping of an underwater robot," in *Proceedings of the 2001 IEEE International Conference on Robotics and Automation*, Seoul, Korea, May 2001, pp. 2767-2772.

[9] S. Negahdaripour, X. Xu, and L. Jin, "Direct estimation of motion from sea floor images for automatic station-keeping of submersible platforms," *IEEE Journal of Oceanic Engineering*, vol. 24, no. 3, pp. 370-382, 1990.

[10] R. Wang, Y. Wang, S. Wang, C. Tang, and M. Tan, "Modular design and control of an underwater biomimetic vehicle-manipulator system," in *Proceedings of the IEEE/RSJ International Conference on Intelligent Robots and Systems Workshop on Robot Modularity*, 2016.

[11] Y. Wang, S. Wang, Q. Wei, M. Tan, C. Zhou, and J. Yu, "Development of an underwater manipulator and its free-floating autonomous operation," *IEEE/ASME Transactions on Mechatronics*, vol. 21, no. 2, pp. 815-824, 2016.

[12] R. Wang and S. Wang, "Design and implementation of a biomimetic underwater propeller with a undulating long fin," *Journal of Huazhong University of Science and Technology (Nature Science Edition)*, vol. 43, no. s1, pp. 408-411, 2015.

[13] R. Wang, Y. Wang, S. Wang, and C. Tang, "Switching control for 3-D way-point tracking of a biomimetic underwater vehicle," in *Proceedings of the 27th International Ocean and Polar Engineering Conference*, San Francisco, California, USA, August 2017.

[14] R. Wang, S. Wang, and Y. Wang, "A hybrid heading control scheme for a biomimetic underwater vehicle," in *Proceedings of the 26th International Ocean and Polar Engineering Conference*, Rhodes, Greece, June 2016, pp. 619-625.

[15] R. Wang, S. Wang, Y. Wang, M. Tan, and J. Yu, "A paradigm for path following control of a ribbon-fin propelled biomimetic underwater vehicle," *IEEE Transactions on Systems, Man and Cybernetics: Systems*, 2017.

[16] S. Wang, Y. Wang, Q. Wei, M. Tan, and J. Yu, "A bio-inspired robot with undulatory fins and its control methods," *IEEE/ASME Transactions on Mechatronics*, vol. 22, no. 1, pp. 206-216, 2017.